PCCP

Ion-ion interactions enhance aluminum solubility in alkaline suspensions of nano-gibbsite (α-$Al(OH)_3$) with sodium nitrite/nitrate

Journal:	*Physical Chemistry Chemical Physics*
Manuscript ID	CP-ART-10-2019-005856.R1
Article Type:	Paper
Date Submitted by the Author:	09-Dec-2019
Complete List of Authors:	Dembowski, Mateusz; Pacific Northwest National Laboratory Snyder, Michelle; Pacific Northwest National Laboratory Delegard, Calvin; TradeWind Services LLC Reynolds, Jacob; Washington River Protection Solutions LLC Graham, Trenton; Pacific Northwest National Laboratory Wang, Hsiu-Wen; Oak Ridge National Laboratory Leavy, Ian; Pacific Northwest National Laboratory Baum, Steven; Pacific Northwest National Laboratory Qafoku, Odeta; Pacific Northwest National Laboratory Fountain, Matthew; Pacific Northwest National Laboratory Rosso, Kevin; Pacific Northwest National Laboratory Clark, Sue; Pacific Northwest National Laboratory Pearce, Carolyn; Pacific Northwest National Laboratory

Ion-ion interactions enhance aluminum solubility in alkaline suspensions of nano-gibbsite (α-$Al(OH)_3$) with sodium nitrite/nitrate

Mateusz Dembowski[†], Michelle M. Snyder[†], Calvin H. Delegard[‡], Jacob G. Reynolds[§], Trent R. Graham[†], Hsiu-Wen Wang[¤], Ian I. Leavy[†], Steven R. Baum[†], Odeta Qafoku[†], Matthew S. Fountain[†], Kevin M. Rosso[†], Sue B. Clark[†], and Carolyn I. Pearce[†]

[†]Pacific Northwest National Laboratory, Richland, Washington 99352, United States
[‡]Trade Wind Services, LLC, Richland, Washington 99352, United States
[§]Washington River Protection Solutions, LLC, Richland, Washington 99352, United States
[¤]Oak Ridge National Laboratory, Oak Ridge, Tennessee 37831, United States

Abstract

Despite widespread industrial importance, predicting metal solubilities in highly concentrated, multicomponent aqueous solutions is difficult due to poorly understood ion-ion and ion-solvent interactions. Aluminum hydroxide solid phase solubility in concentrated sodium hydroxide (NaOH) solutions is one such case, with major implications for ore refining, as well as processing of radioactive waste stored at U.S. Department of Energy legacy sites, such as the Hanford Site, Washington State. The solubility of gibbsite (α-$Al(OH)_3$) is often not well predicted because other ions affect the activity of hydroxide (OH^-) and aluminate ($Al(OH)_4^-$) anions. In the present study, we systematically examined the influence of key anions, nitrite (NO_2^-) and nitrate (NO_3^-) as sodium salts on the solubility of α-$Al(OH)_3$ in NaOH solutions taking care to establish equilibrium from both under- and oversaturation. Rapid equilibration was enabled by use of a highly pure and crystalline synthetic nano-gibbsite of well-defined particle size and shape. Measured dissolved aluminum concentrations were compared with those predicted by an α-$Al(OH)_3$ solubility model derived for simple $Al(OH)_4^-/OH^-$ systems. Specific anion effects were expressed as an enhancement factor (Al_{enhc}) conveying the excess of dissolved aluminum. At 45°C, $NaNO_2$ and $NaNO_3$-containing systems exhibited Al_{enhc} values of 2.70 and 1.88, respectively, indicating significant enhancement. The solutions were examined by Raman and high-field ^{27}Al NMR spectroscopy, indicating specific interactions including $Al(OH)_4^-$-Na^+ contact ion pairing and $Al(OH)_4^-$-NO_2^-/NO_3^- ion-ion interactions. Dynamic evolution of the α-$Al(OH)_3$ particles including growth and agglomeration was observed revealing the importance of dissolution/reprecipitation in establishing equilibrium. These studies indicate that incomplete ion hydration, as a result of the low water activity in these concentrated electrolytes, results in: (i) enhanced reactivity of the hydroxide ion with respect to α-$Al(OH)_3$; (ii) increased concentrations of $Al(OH)_4^-$ in solution; and (iii) stronger ion-ion interactions that act to stabilize the supersaturated solutions. This information on the mechanisms by which α-$Al(OH)_3$ becomes supersaturated is essential for more energy-efficient aluminum processing technologies, including the treatment of millions of gallons of $Al(OH)_4^-$-rich high-level radioactive waste.

Introduction

Predicting metal solubilities in concentrated multicomponent aqueous electrolytes remains a major industrial and technological challenge due to poorly understood ion-ion and ion-water interactions at the molecular-scale. The solubility of aluminum in caustic solutions, where the dominant species is the aluminate anion, $Al(OH)_4^-$, is one classic case of widespread importance. For example, the Bayer process that is used to produce the world's supply of aluminum products (e.g. alumina Al_2O_3 for aluminum metal production) relies on precipitation of the mineral gibbsite (α-$Al(OH)_3$) as an essential intermediate.[1] Milling of aluminum-bearing ore (*bauxite*) starts by its dissolution in caustic soda (NaOH) solutions at temperatures up to 200°C in accordance with **Eq. 1**.

$$Al(OH)_3(s) + OH^-(aq) \leftrightarrow Al(OH)_4^-(aq)$$

The resulting Al-rich solutions are subsequently clarified, cooled, and diluted with water.[2] However, precipitation of the desired α-$Al(OH)_3$ phase is often slow and suffers from low yields – hence the solutions are seeded with α-$Al(OH)_3$ which enhances precipitation to limited extent.[3] This metastability of supersaturated aluminate solutions is well-documented, but the underlying causes related to speciation or distribution of complexed/hydrolyzed species at the molecular-scale are only speculated.[2, 4-6]

Similar concerns pertain to the proposed processing of ca. 200,000 m^3 of caustic aluminum-rich high-level radioactive waste, currently stored in 177 underground tanks at the U.S. Department of Energy's Hanford Nuclear Reservation.[7-8] In these complex multicomponent slurry and supernatant wastes, Al is present due to chemical removal of Al metal cladding from early Hanford fuels, addition of $Al(NO_3)_3$ as a solvent extraction "salting agent" in reduction-oxidation (REDOX) reprocessing operations, and use of $Al(NO_3)_3$ to sequester corrosive fluoride used in dissolution processes.[8-10] Much of this aluminum has precipitated out of aqueous solution as phases such as α-$Al(OH)_3$, and boehmite (γ-AlO(OH)) but there still remains a large dissolved load in the highly concentrated supernatant solutions. Hanford waste exhibits extremely high apparent solubility of Al, with concentrations that are three to ten times higher than in simple solutions at the same NaOH concentration.[4] These elevated Al concentrations have been previously assumed to be the result of slow precipitation kinetics.[11] However, a recent study verified that α-$Al(OH)_3$ was three times more soluble in Hanford waste (with the presence of other solute species) than in comparable NaOH concentrations, which suggests that while kinetics play a role, there is a real but yet unclear counterion effect leading to the observed thermodynamic effect.[12]

The concept of specific interactions enhancing solubilities in aqueous solutions has been known for nearly 100 years.[13] Since its development, specific ion interactions have been included in numerous solubility models for concentrated aqueous solutions.[14] They are generally

integrated as empirical interaction factors between components in solution or as formation of ion-pairs for particularly strong interactions. Although the phase equilibria and solubility calculations are inextricably linked to ion pairing, redox reactions, complexation and other phenomena at molecular-scale, many systems can be modeled just as well by increasing the number of empirically determined interaction parameters including assumed ion pairs in the liquid.[15] Indeed, the large number of empirical parameters in solubility models limits our ability to assign any physical significance to the parameters.[14-15] Consequently, this work represents a combined solubility and spectroscopy study to evaluate underlying physical phenomena.

Although the waste at Hanford is a multi-component mixture of electrolytes, the two most prevalent dissolved species, in addition to sodium hydroxide and aluminate, are sodium nitrite and sodium nitrate. Given the large concentrations of these electrolytes, specific interactions between aluminate and hydroxide with either nitrite or nitrate as well as with added sodium could account for some of the elevated aluminum solubilities observed in Hanford waste. In the current study, we explore the solubility of α-$Al(OH)_3$ in the α-$Al(OH)_3$-NaOH-H_2O system, and methodically assess the influence of $NaNO_2$ and/or $NaNO_3$ by establishing equilibrium from both under- and over-saturation. Measured equilibrium concentrations are compared with the values predicted by solubility models derived for simple sodium aluminate/hydroxide systems validated against α-$Al(OH)_3$ solubility in real and simulated tank waste. The effects of NO_2^- and NO_3^- are represented by a relative enhancement factor (Al_{enhc}) term. High-field ^{27}Al NMR and Raman spectroscopic characterization of the final solutions is used to probe change in Al speciation as a function of the underlying solution chemistry. Additional characterization of solids at equilibrium with the solution confirms that the solid phase remains as α-$Al(OH)_3$, but suggests a dynamic evolution of particle size and morphology. These collective findings provide a quantitative understanding of the effects of NO_2^-, and NO_3^- on the solubility of α-$Al(OH)_3$. This mechanistic information will inform solubility models, allowing the rational design of solution conditions to control aluminum solubility, both for aluminum refining and for the processing of high-level radioactive waste.

Experimental

Synthesis of α-$Al(OH)_3$

Nano-sized α-$Al(OH)_3$ particles (ca. 350 x 35 nm length x width) were synthesized according to procedure described elsewhere.[16] Briefly, a 0.25 mol L^{-1} solution of aluminum nitrate nonahydrate ($Al(NO_3)_3 \cdot 9H_2O$, ≥98%, Sigma-Aldrich) was prepared and titrated using 1.0 mol L^{-1} sodium hydroxide (NaOH, ≥98%, Sigma-Aldrich) to reach a pH of 5. The resulting precipitates were stirred at room temperature for one hour and collected by centrifugation. Three H_2O (18 MΩ-cm) wash/centrifugation cycles were performed to remove residual Na^+ and NO_3^- ions. The washed precipitate was re-dispersed in H_2O, transferred to a Teflon autoclave, sealed in a Parr bomb, and heated (80°C) in an electric oven equipped with a rotating element

(ca. 10 rpm) for 96 hours. Resulting α-$Al(OH)_3$ particles were harvested by centrifugation and subject to the same triple H_2O wash/centrifugation cycle prior to drying in an oven at 50°C overnight. The identity of α-$Al(OH)_3$ was confirmed before and after the dissolution experiments using powder X-ray diffraction (PXRD). No secondary Al-containing phases were detected (see **Supporting Information**).

Solubility Experiments

All solubility experiments were conducted in triplicate, in sealed Teflon tubes, and in an argon-filled glove box to minimize CO_2 capture by concentrated NaOH solutions. Experiments to determine Al solubility by approaching equilibrium from undersaturation were conducted by adding 0.304 – 2.614 g of nano-platelet α-$Al(OH)_3$ to 13 mL of solution containing varying concentrations of NaOH solution and added $NaNO_3$ (Fisher Scientific, >99%) and/or $NaNO_2$ (Fisher Scientific, >97%) (**Table 1**). H_2O (18 MΩ-cm) used in the solubility experiments was boiled and degassed prior to use. Given that high quantities of $NaNO_3$ and/or $NaNO_2$ used in the solubility experiments, the starting solutions were analyzed by ion chromatography (IC) for the presence of possible impurities; chloride (< 250 ppm), bromide (< 500 ppm), fluoride (< 100 ppm), phosphate (< 750 ppm), and sulfate (< 750 ppm) were all below their estimated quantitation limits. Teflon tubes containing the solutions were placed in aluminum blocks on a stirrer hot plate set at 45°C and stirred using Teflon stir bars at a speed of 600 rpm. The temperature in the blocks was monitored with a thermometer (±0.1°C). Experiments to determine Al solubility by approaching equilibrium from oversaturation were conducted by adding excess nano-platelet α-$Al(OH)_3$ (ca. 1.5-times the expected solubility at 45°C, see **Supporting Information** for solubility model details) to the NaOH solution and heating overnight to 80°C until a clear solution was obtained (**Table 1**). These supersaturated solutions were subsequently cooled to 45°C (indicated as 80 $\rightarrow$ 45°C) and allowed to approach equilibrium. After ≥49 days at 45 °C, seed crystals of nano-platelet α-$Al(OH)_3$ starting material (0.4 g) were added to the oversaturation tests to promote α-$Al(OH)_3$ precipitation. Samples of the solutions (300 µL) were taken periodically and rapidly dispensed through pre-heated 13-mm diameter 0.2-µm pore size polyvinylidene difluoride syringe filters. The filtrate was subsequently diluted with 2% HNO_3 (Optima trace metal grade, Fisher Scientific), and the resulting acidic solution was analyzed within 24 hours by inductively coupled plasma optical emission spectrometry (ICP-OES) for Al concentration. The complex nature of the resulting solutions precluded the use of gravimetric or volumetric methods for determining solubility.[17] Density was determined gravimetrically using known aliquot volume. Once equilibrium was reached, the final sample was also analyzed by IC for NO_2^- and NO_3^- concentrations and total alkalinity was measured for OH^- concentrations (see **Supporting Information** for additional details). The tests are abbreviated as aX^Y or bX^Y, where *a* and *b* represent tests performed from under-, and oversaturation, respectively, *X* represents the experiment number (1-5), and *Y* indicates the identity of the additional salt, other than sodium

hydroxide (NaOH) (e.g. $a1^{NO_2}$, **Table 1**). At the end of contact times, the resulting solids were collected by vacuum filtration through a PYREX Buchner filter funnels with fine fritted glass filters (4 to 6 μm), washed with absolute alcohol, and dried in air at 50°C. A complementary set of experiments conducted from undersaturation at 27°C were carried out to confirm temperature-independence of observed solubility trends (see **Supporting Information**).

Table 1. Mass based composition of stock solutions and the average mass of α-$Al(OH)_3$ used in triplicate experiments (per 13 mL of stock solution)

Exp.	NaOH (g)	$NaNO_2$ (g)	$NaNO_3$ (g)	H_2O (g)	$Al(OH)_3$ (g)	Temp. (°C)
a1	4.051	58.199	0	99.374	0.304	45
a2	4.047	0	53.200	98.688	0.304	45
a3	16.066	34.589	42.972	99.735	1.605	45
a4	24.266	0	0	99.337	2.614	45
b1	4.040	60.944	0	99.837	0.309	80 → 45
b2	4.010	0	52.483	100.325	0.304	80 → 45
b3	16.014	34.916	43.994	99.461	1.601	80 → 45
b4	24.180	0	0	99.334	3.398	80 → 45

Solid Phase Characterization

Powder X-ray diffraction patterns were collected on a Phillips diffractometer equipped with a graphite post-diffraction monochromator and a CuKα X-ray source (λ = 1.5406 Å). Finely ground samples were loaded into zero-background holders and data were taken from 10 to 80 degrees 2-theta. Phase identification was carried out using JADE software in conjunction with ICDD database, which includes the Inorganic Crystal Structure Database. Scanning electron micrographs were collected using a Helios NanoLab 600i SEM (FEI, Hillsboro, OR). A thin carbon film (ca. 10 nm) was sputter coated on each sample prior to imaging. Additional instrumental details and procedures for nuclear magnetic resonance (NMR, MAS-NMR), Brunauer-Emmett-Teller (BET) specific surface area measurements, and Raman spectroscopy are available in **Supporting Information**.

Results

α-$Al(OH)_3$ characterization

The purity of the α-$Al(OH)_3$ utilized in solubility measurements was confirmed using X-ray diffraction (XRD). The calculated and observed background-subtracted XRD patterns are shown in **Figure 1** where α-$Al(OH)_3$ (gibbsite, ICDD ID: 04-011-1369) was the only identifiable crystalline phase. ^{27}Al magic angle spinning (MAS) NMR spectra collected on the starting material confirm the purity of the α-$Al(OH)_3$. The asymmetric ^{27}Al resonance observed at ca. 9.5 ppm corresponds to two unique octahedrally coordinated Al sites present in the crystal structure of α-$Al(OH)_3$ and

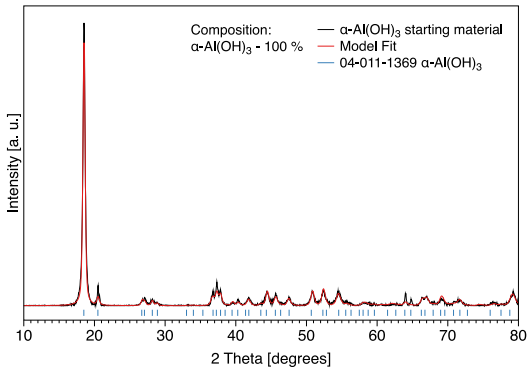

Figure 1. Experimental (black) and model (red) powder X-ray diffraction patterns of the α-$Al(OH)_3$ nano-particles used in solubility measurements.

is consistent with prior literature reports (**Figure S1**).[18-21] The presence of trace amorphous Al gel, or undercoordinated surface sites can be ruled out due to lack of signals in the 40 and 70 ppm regions corresponding to five- and four-coordinate Al, respectively.[22-25] The morphology, dispersity and approximate dimensions of as synthesized material were evaluated using scanning electron microscopy (SEM) (**Figure 2**, top). An estimate of particle size from the SEM micrographs indicated an average particle length and thickness of 347±74 and 35±14 nm, respectively (**Figure 2**, bottom). The Brunauer-Emmett-Teller (BET) specific surface area for α-$Al(OH)_3$ starting material was 32.5 m^2/g. These sub-micron, high surface area particles were selected to enhance dissolution rates and shorten the time required to reach equilibrium.

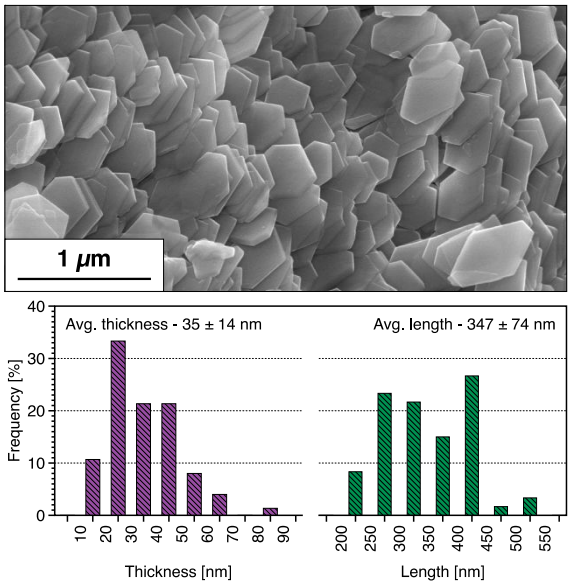

Figure 2. (top) SEM micrograph of the as-synthesized α-$Al(OH)_3$ used in solubility experiments showing euhedral, hexagonal plate-like morphology. (bottom) Histogram of the length and thickness of the as-synthesized α-$Al(OH)_3$.

Attainment of equilibrium from under- and oversaturation

Equilibrium aluminum (Al) concentrations were established to determine the solubility of α-$Al(OH)_3$ in the different solutions (**Table 1**). ICP-OES results are summarized in **Figure 3**. Al concentrations for the 45°C tests obtained from undersaturation (i.e. determined by dissolution of excess α-$Al(OH)_3$) increased gradually to reach steady-state by 21 ($a1^{NO_2}$, $a2^{NO_3}$, and $a3^{NO_2/NO_3}$) and 35 (a4) days. All systems remained stable until completion of sampling at 81 days with average Al concentration plateau values of 0.176±0.007 mol L^{-1} for $a1^{NO_2}$, 0.145±0.007 mol L^{-1} for $a2^{NO_3}$, 0.751±0.040 mol L^{-1} for $a3^{NO_2/NO_3}$, and 1.009±0.046 mol L^{-1} for a4.

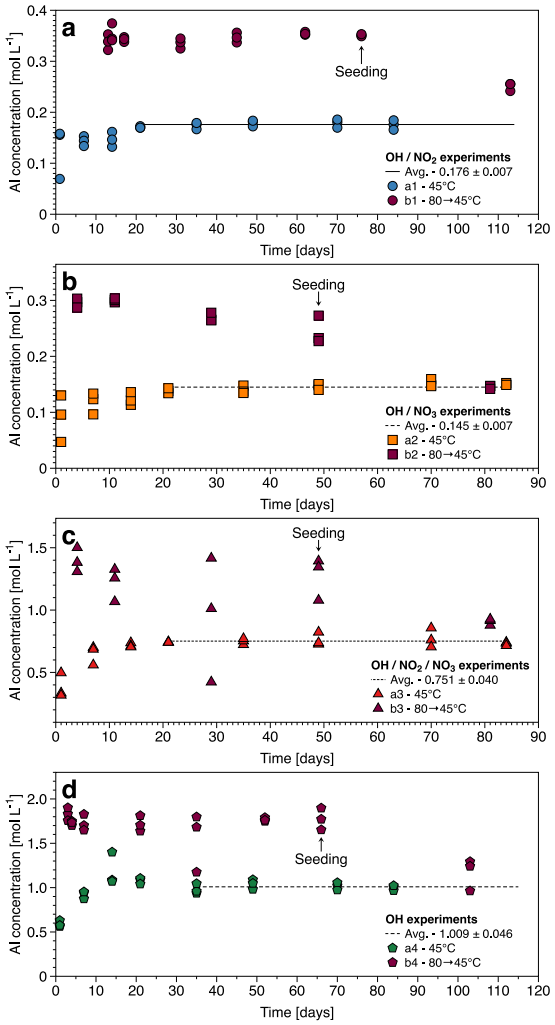

Figure 3. Al concentrations versus reaction time for tests **(a)** a1 and b1 (OH^-/NO_2^-), **(b)** a2 and b2 (OH^-/NO_3^-), **(c)** a3 and b3 ($OH^-/NO_2^-/NO_3^-$), and **(d)** a4 and b4 (OH^-). Addition of α-$Al(OH)_3$ seed crystals is indicated with an arrow. Horizontal lines represent the average Al concentrations obtained from undersaturation.

Solubility tests from oversaturation with the same initial solution compositions to $a1^{NO_2}$ ($b1^{NO_2}$), $a2^{NO_3}$ ($b2^{NO_3}$), $a3^{NO_2/NO_3}$ ($b3^{NO_2/NO_3}$), and a4 (b4) were carried out. For tests $b1^{NO_2}$ and b4 (**Figure 3a**, **d**), no crystallization or decrease in Al concentration was observed in any of the triplicates prior to the addition α-$Al(OH)_3$ seed crystals (seeding denoted by arrow). For test $b2^{NO_3}$,

two of the triplicates developed turbidity after 49 days, accompanied by ca. 15% decrease in Al concentration, compared with the triplicate that showed no obvious crystallization (**Figure 3b**). For test $b3^{NO_2/NO_3}$ one of the triplicates developed turbidity after 49 days, accompanied by ca. 21% decrease in Al concentration compared with the two triplicates that showed no obvious crystallization. These results highlight that the oversaturated solutions are thermodynamically unstable, and small fluctuations in solution conditions between the triplicate samples can be enough to overcome the kinetic barrier to crystallization.[5] After 76, 49, 49, and 66 days, respectively, α-$Al(OH)_3$ seed crystals were added to $b1^{NO_2}$, $b2^{NO_3}$, $b3^{NO_2/NO_3}$, and b4 samples (**Figure 3**, arrows) resulting in Al concentrations matching (or approaching) those attained within the similar 20-30 days for the tests from undersaturation. To confirm that α-$Al(OH)_3$ remained the solubility controlling phase after exposure to elevated temperature, the residual solids were harvested by vacuum filtration and characterized by PXRD and SEM.

The effect of temperature and anion concentration on particle morphology and surface area

PXRD analysis confirmed retention of the original α-$Al(OH)_3$ phase as the only Al bearing species (see **Supporting Information**). Residual $NaNO_2$ and/or $NaNO_3$ phases were present due to use of ethanol during the harvesting and washing steps. SEM analysis of the α-$Al(OH)_3$ phase after reaction showed clear changes to the particle size and morphology, particularly following seeding of oversaturated solutions. The changes were likely the result of either growth (*via* oriented attachment, or Ostwald ripening), or re-precipitation/nucleation.

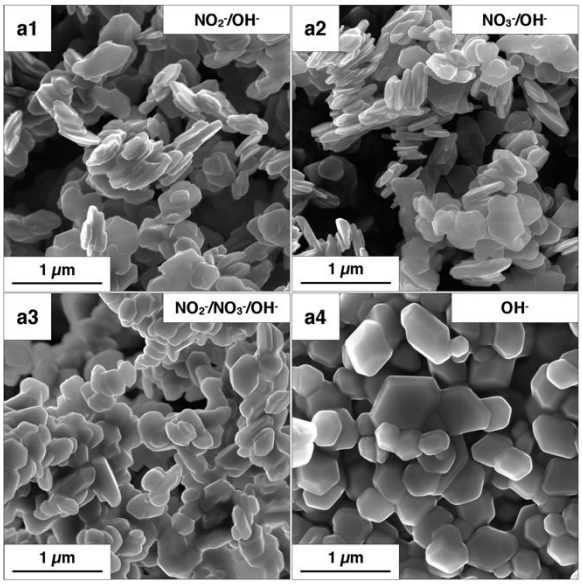

Figure 4. SEM micrographs of α-$Al(OH)_3$ solids harvested at the end of 45°C (undersaturation) solubility experiments.

Select SEM micrographs are shown in **Figure 4** and **5**. The solid phases extracted from suspensions in which equilibrium was obtained from undersaturation (a1-4) show minimal alteration of the initially euhedral, hexagonal plates, despite long contact time (up to 81 days)

and constant agitation (**Figure 4**). Partial dissolution of the starting phase is evident from presence of small, irregular particles (< 200 nm) and rounded edges when compared to the starting material (**Figure 2**). New {1 0 1}, and {1 1 2} chamfered faces are noted in particles extracted from a3$^{NO_2/NO_3}$ and a4 experiments.[26] Particles extracted from suspensions in which equilibrium was obtained from oversaturation (b2^{NO_3}, b3$^{NO_2/NO_3}$, and b4) show considerable alteration (**Figure 5**). Particles ca. 1 µm in size assume morphologies ranging from hexagonal prismatic with well-developed basal {0 0 1} and prismatic {1 0 0}, {1 1 0} faces (b2^{NO_3}) to complex, multi-chamfered, and in-grown particles (b3$^{NO_2/NO_3}$ and b4) showing early stages of random agglomeration.[26-27]

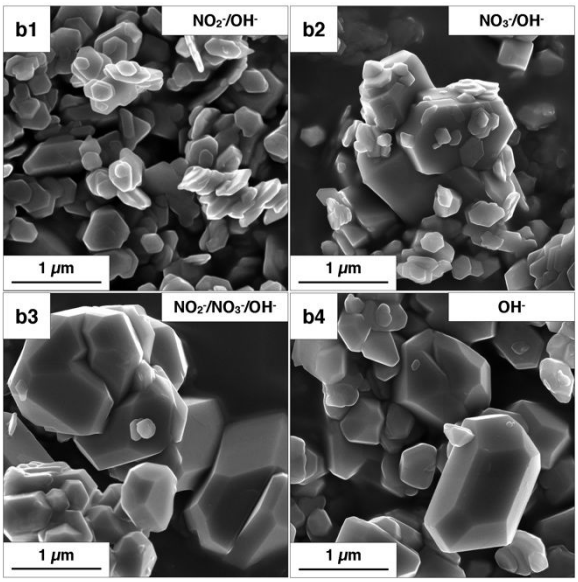

Figure 5. SEM micrographs of α-Al(OH)$_3$ solids harvested at the end of 80 → 45°C (oversaturation) solubility experiments.

The high surface area of the starting material (32.5 m^2/g) paired with SEM micrographs suggests that the 45°C experiments attained equilibrium from undersaturation mainly by means of particle dissolution, although tests a3$^{NO_2/NO_3}$ and a4 exhibited particles with new chamfered faces (**Figure 4**) consistent with particle growth/re-precipitation. Oversaturation experiments demonstrate that introduction of high-surface area seed crystals induces growth/precipitation resulting in formation of ca. 1 µm sized particles with well-developed, euhedral faces (**Figure 5**).

Spectroscopic characterization of aluminate solutions

Identifying and understanding the interactions between species present in caustic aluminate solutions is central to advancement of predictive models. To gain insights into the chemistry of the α-Al(OH)$_3$-NaOH-H$_2$O system in the presence and absence of $NaNO_2$ and/or $NaNO_3$, Raman and ^{27}Al NMR spectra were collected at the end of the experiments. **Figure 6** shows Raman spectra of the a1-4 solutions, highlighting the positions of the symmetrical

vibration of the $Al(OH)_4^-$ (ca. 625 cm^{-1}), and the bending modes of NO_3^- (ca. 724 cm^{-1}) and NO_2^- (ca. 822 cm^{-1}). The position of the $Al(OH)_4^-$ signal (> 624 cm^{-1}) indicates presence of a Na^+…$Al(OH)_4^-$ contact ion pair (CIP) as solvent separated ion pair (SSIP) are commonly observed at 620 cm^{-1}.[2] The constant position of the $Al(OH)_4^-$ band in **Figure 6** (625 cm^{-1}) indicates that the aluminate-cation interactions remain unchanged, despite the significant disparities in solution composition. Notably, no signals are observed in the 500-700 cm^{-1} spectral window that would indicate presence of significant quantities of dimeric aluminate species (e.g. $Al_2O(OH)_6^{2-}$).[28-30] The lack of a signal at 724 cm^{-1} in the Raman spectrum of $a1^{NO_2}$ (**Figure 6**), combined with ion chromatography results (**Table 2**), indicates that no oxidation of NO_2^- took place under considered experimental conditions.

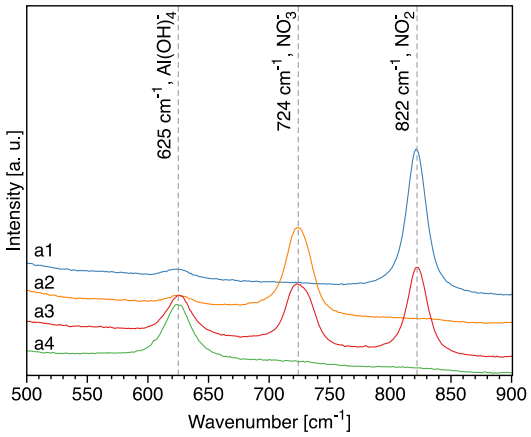

Figure 6. Raman spectra of the a1-4 solutions at the end of contact time showing signals corresponding to the aluminate ion (625 cm^{-1}), nitrate ion (724 cm^{-1}), and nitrite ion (822 cm^{-1}).

High-field ^{27}Al NMR spectra of solutions at the end of the experiments are summarized in **Figure 7**. Use of a physically separated, coaxial insert containing an internal standard (1 mol L^{-1} $Al(NO_3)_3$ in H_2O, δ = 0 ppm, see **Supporting Information**) allowed for precise and accurate determination of $Al(OH)_4^-$ chemical shifts that range from ca 79.583±0.015 to 80.697±0.007 ppm. Nitrite containing systems (blue circles) exhibit the most downfield chemical shifts with respect to hydroxide only systems (green pentagons). Prior literature reports indicate that increasing OH^- concentrations (at constant Al concentration) result in an upfield chemical shift, and increasing Al concentration (at constant OH^- concentration) results in a downfield chemical shift, of the ^{27}Al signal.[31] Although the observed trend in ^{27}Al NMR chemical shifts ($a1^{NO_2}$>$a2^{NO_3}$>$a3^{NO_2/NO_3}$>a4) is in agreement with literature trends, the span of observed chemical shifts ($a1^{NO_2}$ and a4, Δδ = 1.1 ppm) is anomalously high considering that chemical shifts of aluminate solutions characterized by NaOH concentrations of less than 5 mol L^{-1} are expected to be independent of Al concentration.[2, 31] Detailed interpretation of literature trends is challenging as at extreme limits, both the increase of [Na] at low [Al], as well as increase of [Al] at constant [Na], result in higher probability of SSIP or CIP formation.[2, 6, 31] Taking into account the constant position of the

symmetrical vibration of the $Al(OH)_4^-$ in these solutions determined by Raman spectroscopy (**Figure 6**) the significant downfield shift of ^{27}Al signals in the presence of $NaNO_2$ and/or $NaNO_3$ likely arises due to a number of possible anion-cation ($Al(OH)_4^-$…Na^+), and/or anion-anion (e.g. $Al(OH)_4^-$…$Al(OH)_4^-$, $Al(OH)_4^-$…NO_2^-) interactions, the latter of which has been observed and extensively studied in phosphate-based systems amongst others.[32-34]

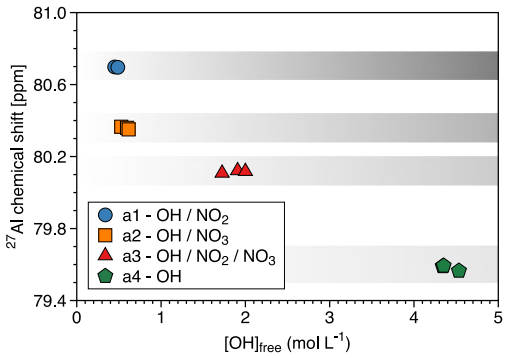

Figure 7. High-field ^{27}Al NMR spectra of internally referenced 12 tests solutions showing the chemical shift as a function of free hydroxide concentration and solution composition.

Measured, predicted, and literature values of α-Al(OH)$_3$ solubility

Equilibrium Al concentrations were compared with results obtained from a new calculation for α-$Al(OH)_3$ solubility, made using the Pitzer virial-coefficient approach and literature data for activity coefficient corrections and interaction parameters.[6] Results are discussed in terms of molality (m, mol kg^{-1}), calculated using measured equilibrium concentrations of OH^-, NO^{2-}, and NO^{3-} (**Table 2**), as differences in density of the concentrated $NaNO_2$/$NaNO_3$ solutions can be superimposed on observed thermodynamic differences.

Equilibrium thermodynamics calculations were performed using the PHREEQC software package (version 3) that augments the default Pitzer database and our tabulated data block to include α-$Al(OH)_3$ equilibrium constants and Pitzer parameters best selected from the literatures.[35] This extended Pitzer database was discussed in detail and used previously in our two related works.[6, 36] For demonstration, we provide an example of PHREEQC input file (see **Supporting Information**) for the calculation of α-$Al(OH)_3$ solubility in NaOH-H_2O system at 45°C. Comparison of the current model against literature α-$Al(OH)_3$ solubility across a range of temperatures in the NaOH-H_2O system shows good agreement (**Supporting Information**). The calculated solubility curve of α-$Al(OH)_3$ at 45°C is illustrated in **Figure 8** as a function of increasing alkaline concentrations. Here, the notional free hydroxide ion concentration, $[OH^-]_{free}$, is defined as $[OH^-]_{free} = [NaOH]_{total} - [Al^{3+}]_{total}$ (the subscript total denotes analytical or total concentration), and $[OH^-]_{free}$ represents the actual free hydroxide ion concentration if the only significant aluminum-containing complex in solution is $Al(OH)_4^-$. Same definition also applies to the systems containing additional NO_2^- and/or NO_3^- species.

Table 2. Average solution temperatures, densities, solute concentrations (in mol kg^{-1}), and enhancement factors, Al_{enhc} at the final sampling

Exp.	$[OH^-]_{free}$ (m)	[Al] (m)	$[NO_2^-]$ (m)	$[NO_3^-]$ (m)	Density (g/cm^3)	Avg. Al_{enhc}[a]	Temp (°C)
a1	0.620±0.029	0.230±0.012	9.963±0.133	0	1.326±0.007	2.70	43.3
a2	0.701±0.059	0.181±0.002	0	6.368±0.220	1.316±0.013	1.88	43.3
a3	2.488±0.223	0.968±0.044	4.673±0.170	4.529±0.156	1.451±0.017	2.42	43.3
a4	4.627±0.087	1.047±0.034	0	0	1.248±0.009	1.06	43.3
b1	0.924±0.022	0.363±0.011	13.025±0.181	0	1.368±0.008	2.80	80 → 46.8
b2	0.698±0.014	0.169±0.003	0	5.630±0.182	1.311±0.003	1.76	80 → 45.2
b3	2.435±0.140	1.254±0.029	5.209±0.046	4.913±0.050	1.463±0.006	3.21	80 → 45.2
b4	4.760±0.249	1.253±0.211	0	0	1.248±0.013	1.21	80 → 46.8

[a] $Al_{enhc}=[Al]_{meas}/[Al]_{pred}$ where $[Al]_{pred}$ correspond to the Pitzer predicted [Al] concentration at observed $[OH]_{free}$.

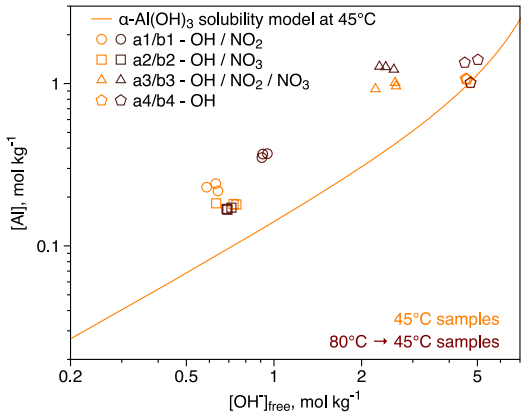

Figure 8. Measured α-$Al(OH)_3$ solubility in current experiments versus solubility predicted from Pitzer model in the system of α-$Al(OH)_3$-NaOH-H_2O.

To compare solubility trends between systems containing only OH^- and systems containing various amounts of $NaNO_2$ and/or $NaNO_3$, the experimentally measured concentrations were divided by those predicted by the α-$Al(OH)_3$ solubility model to calculate enhancement factors for aluminum (Al_{enhc}) (**Table 2**). Higher solubility of α-$Al(OH)_3$ in systems containing $NaNO_2$ and/or $NaNO_3$ is apparent from the Al_{enhc} values of 2.70, 1.88, and 2.42 for the Al solubility attained in $a1^{NO_2}$, $a2^{NO_3}$, and $a3^{NO_2/NO_3}$, respectively. Additional inspection of these results indicate that α-$Al(OH)_3$ solubility is not solely influenced by the ionic strength of the system (i.e. Na^+ concentration), as Al_{enhc} value for $a1^{NO_2}$ (9.5 mol kg^{-1} Na^+) is higher than in $a2^{NO_3}$ (7.4 mol kg^{-1} Na^+), or $a3^{NO_2/NO_3}$ (14.1 mol kg^{-1} Na^+). This implies that the anion (NO_2^- or NO_3^-) has a greater influence on the enhancement of α-$Al(OH)_3$ solubility. Furthermore, for experiments

approached from undersaturation the addition of NO_2^- to the α-$Al(OH)_3$-NaOH-H_2O system results in the highest α-$Al(OH)_3$ solubility enhancement (as $Al(OH)_4^-$) followed by the addition of both NO_2^- and NO_3^-, with addition of only NO_3^- showing the lowest Al_{enhc} values (**Table 2**). Higher Al_{enhc} observed in NO_2^- system can, in part, be the result of its higher solubility as compared to NO_3^-. Addressing the relative enhancement as a function of anion identity requires further investigation. It is worth noting that the system containing NO_2^- approached from supersaturation, despite addition of seed crystals and prolonged aging, exhibited slightly elevated Al concentrations in solution (**Figure 3a**). This is reflected in the Al_{enhc} value of 2.80, as compared to 2.70 for a1 (undersaturation). Similar discrepancy is noted for experiment b3. The reason for stability of supersaturated aluminate solutions is a topic of ongoing studies. A set of complementary 27°C experiments conducted from undersaturation and resulting equilibrium Al concentrations were compared against the current model (see **Supporting Information**). Calculated Al_{enhc} values of 2.56, 1.80, and 2.61 (at 27°C) corresponding to experiments conducted in the presence of NO_2^-, NO_3^-, and both NO_2^- and NO_3^-, respectively, confirm that the identity of the anion plays a critical role in the solubility enhancement across a wide range in temperature.

Discussion

In order to understand the mechanisms by which α-$Al(OH)_3$ becomes supersaturated in these concentrated systems, the effect of low water content on the speciation of the different ions in the system must be considered. Thermodynamics of solutions comprised of monovalent ions at the dilute limit ($[M^+] < 0.1$ m) are well described by the Debye-Hückel equation.[37] Such systems contain an excess of 270 water molecules per ion affording complete solvation of ionic species. However, as the concentration of solutes increases, ion-ion interactions become an important consideration. Specifically, the solutions studied here are characterized by five or fewer water molecules per ion, suggesting that archetypal solvation environment of OH^- (four water molecules), $Al(OH)_4^-$ (five water molecules), Na^+ (five to six water molecules), NO_2^- and NO_3^- (six water molecules) can no longer be satisfied.[38-42] Indeed, shifts in the wavelength of the $Al(OH)_4^-$ band in the Raman spectra for all of the solutions studied here indicate formation of $Al(OH)_4^-$ contact ion pairs, consistent with the lack of water to coordinate the ions in these highly concentrated, solvent-deprived systems (**Figure 6**).

Given that OH^- is solvated by the fewest number of water molecules, it is likely that this ion will be most affected when there are insufficient water molecules to fill the first solvation shell. Studies of hydroxide ion solvation in NaOH solutions show that at high concentration (≥6 m), the number of H_2O molecules that are H-bonded to OH^- (via hydroxyl O atom) in the first solvation shell decreases from four to three.[43-44] From computational studies, this change in solvation structure occurs when the H_2O:NaOH ratio drops below eight, corresponding to four or fewer water molecules per ion, and is concurrent with formation of H-bonded OH^--OH^- and Na^+-Na^+ moieties.[45-47] The change in hydration number of OH^- is reflected in the physical properties

of concentrated NaOH solutions, with considerable differences in the slope of the viscosity, electrical conductivity, and partial molal heat capacities noted as their water content decreased below ca. nine to eight water molecules per mole of NaOH (ca. four waters per OH^-).[48] Analogous deviations were noted in water activity trends and the mechanism of proton transfer.[37, 45] Thus, it can be expected that this change in hydration number for OH^- will also affect its reactivity with respect to the dissolution and precipitation of α-$Al(OH)_3$ under caustic conditions, in accordance with **Eq. 1**.

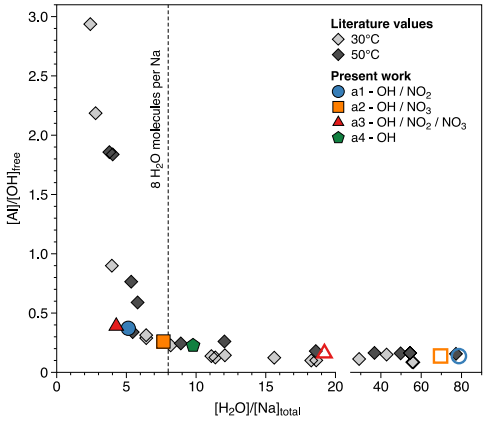

Figure 9. Comparison of literature values for the H_2O:Na molal ratio at equilibrium with α-$Al(OH)_3$ with present work. Unfilled blue circle, orange square, and red triangle symbols represent the predicted ratios for $a1^{NO2}$, $a2^{NO3}$, and $a3^{NO2/NO3}$ experiments without added NO_2^- and/or NO_3^-, respectively.

Figure 9 shows the Al:OH mole ratio at equilibrium with α-$Al(OH)_3$ as a function of H_2O:Na^+ mole ratio, for the α-$Al(OH)_3$-NaOH-H_2O system at 30, 45 and 50°C.[49-53] The solubility of α-$Al(OH)_3$ is relatively low (<0.5 mol Al/mol OH) when the H_2O:Na^+ mole ratio is high, but there is a sharp transition to significantly higher α-$Al(OH)_3$ solubility when the system contains fewer than about eight mol of water per mol of NaX (i.e., four water molecules per ion, X = OH^-, NO_2^-, NO_3^-, or $Al(OH)_4^-$) (denoted by the dashed line in **Figure 9**). Notably, addition of sodium nitrite and/or nitrate in the present study reduces the available hydration number per NaX from ca. 79 to five for $a1^{NO_2}$, 70 to eight for $a2^{NO_3}$, and 19 to four for $a3^{NO_2/NO_3}$ compared to systems defined by the same hydroxide content (**Figure 9**, unfilled vs. filled points). Thus, the addition of NO_2^- and NO_3^- comes at the substantial expense of remaining available H_2O, triggering new system properties arising from under-solvation of the OH^- anion, leading to enhanced α-$Al(OH)_3$ solubility.

That these conditions uniquely favor enhanced solubilization of $Al(OH)_4^-$ may be due to its greater ability to partake in anion specific interactions relative to OH^-, including the prospect of forming multinuclear species.[28-29, 54] The evidence for this is provided in part by a shift in the $Al(OH)_4^-$ band in the Raman spectra, indicating formation of $Al(OH)_4^-$ contact ion pairs, and in part by the change in ^{27}Al NMR chemical shift, which shows progressive de-shielding of the ^{27}Al

nucleus in systems containing NO_3^- and NO_2^-. As current experimental parameters preclude determination of solubility enhancement as a function of anion identity (NO_2^- vs. NO_3^-), the reason for why nitrite should have a larger effect than nitrate remains unclear; at more dilute conditions their affinities for and numbers of waters of solvation remain a matter of ongoing debate, though their tendencies to form contact ion pairs with Na^+ are thought to be similar.[55] The observed effect may therefore have more to do with their relative solubility in complex multicomponent mixtures and propensities for anion-anion interactions, a less explored topic deserving of future research. This reinforces the broader finding that the observed solubility enhancement of α-$Al(OH)_3$ and stabilization of $Al(OH)_4^-$ is achieved through specific anion interactions, the details of which depends on the nature of the anion.

Conclusions

Motivated by the poorly understood excess Al concentrations in low water, highly concentrated NaOH radioactive waste solutions stored at DOE legacy sites, the present study sought to determine if enhanced α-$Al(OH)_3$ solubility and $Al(OH)_4^-$ ion-pairing can also be induced at lower OH^- concentrations by replacing H_2O with other relevant highly soluble salts of $NaNO_2$ or $NaNO_3$.

α-$Al(OH)_3$ equilibrated with modest quantities of NaOH in highly concentrated solutions of $NaNO_2$ or $NaNO_3$ limited the solvent content to less than four H_2O molecules per dissolved ion. Equilibrium concentrations of Al in the α-$Al(OH)_3$-NaOH-H_2O system, in the presence and absence of $NaNO_2$ and/or $NaNO_3$, were determined from both under- and oversaturation at 45°C. In the absence of added $NaNO_2$ or $NaNO_3$, measured Al concentrations agreed well with predictions from a new α-$Al(OH)_3$ solubility model based on Pitzer virial-coefficients. α-$Al(OH)_3$ particle coarsening and agglomeration were evident, consistent with dissolution/reprecipitation during equilibration. Both nitrite and nitrate enhanced α-$Al(OH)_3$ solubility above that expected for solutions without the additional salts but with the same hydroxide molality. The enhancement does not scale with NO_2^-/NO_3^- concentration, thus appears dependent less on ionic strength and more on anion identity.

Concentrated NaOH solutions (> 8 molal) only have enough solvent for ca. 3.5 water molecules per dissolved ion, resulting in a transition in the coordination number for OH^- from four H-bonded H_2O molecules to three. In the α-$Al(OH)_3$-NaOH-H_2O system, this is concurrent with a change in the ^{27}Al chemical shift in NMR spectra, and in the wavelength of the $Al(OH)_4^-$ band in Raman spectra, caused by inner sphere ion-pairing between $Al(OH)_4^-$ ions, and with Na^+ ions, in these solutions. Similarly, Raman spectroscopy and high-field ^{27}Al NMR measurements performed here on NO_2^-/NO_3^--containing systems provide evidence for anion-anion interactions between $Al(OH)_4^-$ and with NO_2^-/NO_3^-, which collectively act to stabilize the higher concentrations of $Al(OH)_4^-$ in solution.

Our findings confirm that the high solubility of α-$Al(OH)_3$ observed in low water environments is caused by the change in ion speciation imposed by the H_2O deficit, which favors $Al(OH)_4^-$ in solution relative to under-solvated OH^-. This change is insensitive to the cause of the low water environment, occurring both in high concentrations of NaOH, or in lower concentrations of NaOH with the addition of other electrolytes like $NaNO_2$ or $NaNO_3$. The effect can easily double the solubility of α-$Al(OH)_3$ in high pH solutions, likely contributing to but not fully accounting for the three to tenfold solubility increase observed for the caustic radioactive wastes. More research is needed to fully unravel the ion pairing interactions that dominate these complex low water activity solutions.

Acknowledgements

The synthesis and solid phase characterization of the nano-sized α-$Al(OH)_3$ particles, along with the writing of this manuscript, were supported as part of IDREAM (Interfacial Dynamics in Radioactive Environments and Materials), an Energy Frontier Research Center funded by the U.S. Department of Energy (DOE) Office of Science, Basic Energy Sciences. The solubility tests in this work were completed in support of the One System River Protection Project Integrated Flowsheet. Funding for these tests came from Washington River Protection Solutions. Solid phase characterization of the nano-sized α-$Al(OH)_3$ particles and solution characterization via Raman spectroscopy was performed using the Environmental Molecular Sciences Laboratory (EMSL, grid.436923.9), a national scientific user facility sponsored by the DOE's Office of Biological and Environmental Research located at Pacific Northwest National Laboratory (PNNL) under proposal number 49771. PNNL is a multiprogram national laboratory operated for DOE by Battelle Memorial Institute under Contract No. DE-AC05-76RL0-1830.

References:

(1) Hind, A. R.; Bhargava, S. K.; Grocott, S. C., The Surface Chemistry of Bayer Process Solids: A Review. *Colloid. Surface A* **1999,** *146*, 359-374.

(2) Sipos, P., The Structure of Al(III) in Strongly Alkaline Aluminate Solutions - A Review. *J. Mol. Liq.* **2009,** *146*, 1-14.

(3) Den Hond, R.; Hiralal, I.; Rijkeboer, A., Alumina Yield in the Bayer Process Past, Present and Prospects. In *Essential Readings in Light Metals: Volume 1 Alumina and Bauxite*, Donaldson, D.; Raahauge, B. E., Eds. Springer International Publishing: Cham, 2016; pp 528-533.

(4) Reynolds, J. G., The Apparent Solubility of Aluminum(III) in Hanford High-Level Waste Tanks. *J. Environ. Sci. Health Part A* **2012,** *47*, 2213-2218.

(5) Vrbaski, T.; Ivekovic, H.; Pavlovic, D., The Spontaneous Precipitation of Hydrated Alumina from Aluminate Solutions. *Can. J. Chem.* **1958,** *36*, 1410-1415.

(6) Graham, T. R.; Dembowski, M.; Martinez-Baez, E.; Zhang, X.; Jaegers, N. R.; Hu, J. Z.; Gruszkiewicz, M. S.; Wang, H. W.; Stack, A. G.; Bowden, M. E.; Delegard, C. H.; Schenter, G. K.; Clark, A. E.; Clark, S. B.; Felmy, A. R.; Rosso, K. M.; Pearce, C. I., In Situ Al-27 NMR Spectroscopy of Aluminate in Sodium Hydroxide Solutions above and below Saturation with Respect to Gibbsite. *Inorg. Chem.* **2018,** *57*, 11864-11873.

(7) Agnew, S. F.; Reynolds, J. G.; Johnston, C. T. In *Aluminum Solubility Model for Hanford Tank Waste Treatment*, 2009 Waste Management Symposium – Proceedings of Waste Management 2009, Waste Management Symposia Inc., Phoenix, AZ, United States, 2009.

(8) Peterson, R. A.; Buck, E. C.; Chun, J.; Daniel, R. C.; Herting, D. L.; Ilton, E. S.; Lumetta, G. J.; Clark, S. B., Review of the Scientific Understanding of Radioactive Waste at the US DOE Hanford Site. *Environ. Sci. Technol.* **2018,** *52*, 381-396.

(9) Krumhansl, J. L.; Brady, P. V.; Zhang, P. C.; Arthur, S.; Hutcherson, S. K.; Liu, J.; Qian, M.; Anderson, H. L., Phase Chemistry and Radionuclide Retention of High-Level Radioactive Waste Tank Sludges. In *Nuclear Site Remediation*, American Chemical Society: 2000; Vol. 778, pp 98-112.

(10) Kupfer, M.; Boldt, A., Standard Inventories of Chemicals and Radionuclides in Hanford Site Tank Wastes. Westinghouse Hanford Company, Richland, WA, United States, **1997**.

(11) Reynolds, J. G.; Reynolds, D. A. *A Modern Interpretation of the Barney Diagram for Aluminum Solubility in Tank Waste*. Waste Management Symposia Inc., Phoenix, AZ, United States, 2009.

(12) Reynolds, J. G.; McCoskey, J. K.; Herting, D. L., Gibbsite Solubility in Hanford Nuclear Waste Approached from above and below Saturation. *Ind Eng Chem Res* **2016,** *55*, 5465-5473.

(13) Brönsted, J. N., Studies on Solubility. IV. The Principle of the Specific Interaction of Ions. *J. Am. Chem. Soc.* **1922,** *44*, 877-898.

(14) May, P. M.; Rowland, D., Thermodynamic Modeling of Aqueous Electrolyte Systems: Current Status. *J. Chem. Eng. Data* **2017,** *62*, 2481-2495.

(15) Sterner, S. M.; Felmy, A. R.; Oakes, C. S.; Pitzer, K. S., Correlation of Thermodynamic Data for Aqueous Electrolyte Solutions to Very High Ionic Strength Using INSIGHT: Vapor Saturated Water Activity in the System $CaCl_2$-H_2O to 250 degrees C and Solid Saturation. *Int. J. Thermophys.* **1998,** *19*, 761-770.

(16) Zhang, X.; Zhang, X. W.; Graham, T. R.; Pearce, C. I.; Mehdi, B. L.; N'Diaye, A. T.; Kerisit, S.; Browning, N. D.; Clark, S. B.; Rosso, K. M., Fast Synthesis of Gibbsite Nanoplates and Process Optimization using Box-Behnken Experimental Design. *Cryst. Growth. Des.* **2017,** *17*, 6801-6808.

(17) Königsberger, E., Editorial: Guildelines for the Measurement of Solid-Liquid Solubility Data at Atmospheric Pressure. *J. Chem. Eng. Data* **2019**, *64*, 381-385

(18) Ashbrook, S. E.; McManus, J.; MacKenzie, K. J. D.; Wimperis, S., Multiple-Quantum and Cross-Polarized Al-27 MAS NMR of Mechanically Treated Mixtures of Kaolinite and Gibbsite. *J. Phys. Chem. B.* **2000,** *104*, 6408-6416.

(19) Chandran, C. V.; Kirschhock, C. E. A.; Radhakrishnan, S.; Taulelle, F.; Martens, J. A.; Breynaert, E., Alumina: Discriminative Analysis Using 3D Correlation of Solid-State NMR Parameters. *Chem. Soc. Rev.* **2019,** *48*, 134-156.

(20) Hu, J. Z.; Zhang, X.; Jaegers, N. R.; Wan, C.; Graham, T. R.; Hu, M.; Pearce, C. I.; Felmy, A. R.; Clark, S. B.; Rosso, K. M., Transitions in Al Coordination during Gibbsite Crystallization Using High-Field Al-27 and Na-23 MAS NMR Spectroscopy. *J. Phys. Chem. C* **2017,** *121*, 27555-27562.

(21) Wimpenny, J.; Colla, C. A.; Yu, P.; Yin, Q. Z.; Rustad, J. R.; Casey, W. H., Lithium isotope fractionation during uptake by gibbsite. *Geochim. Cosmochim. Acta* **2015,** *168*, 133-150.

(22) Casey, W. H., Large Aqueous Aluminum Hydroxide Molecules. *Chem. Rev.* **2006,** *106*, 1-16.

(23) Cui, J. L.; Kast, M. G.; Hammann, B. A.; Afriyie, Y.; Woods, K. N.; Plassmeyer, P. N.; Perkins, C. K.; Ma, Z. L.; Keszler, D. A.; Page, C. J.; Boettcher, S. W.; Hayes, S. E., Aluminum Oxide Thin Films from Aqueous Solutions: Insights from Solid-State NMR and Dielectric Response. *Chem. Mater.* **2018,** *30* (21), 7456-7463.

(24) Swaddle, T. W.; Rosenqvist, J.; Yu, P.; Bylaska, E.; Philiips, B. L.; Casey, W. H., Kinetic Evidence for Five-Coordination in $AlOH_2^+$(aq) ion. *Science* **2005,** *308*, 1450-1453.

(25) Zhang, X.; Huestis, P. L.; Pearce, C. I.; Hu, J. Z.; Page, K.; Anovitz, L. M.; Aleksandrov, A. B.; Prange, M. P.; Kerisit, S.; Bowden, M. E.; Cui, W.; Wang, Z.; Jaegers, N. R.; Graham, T. R.; Dembowski, M.; Wang, H.-W.; Liu, J.; N'Diaye, A. T.; Bleuel, M.; Mildner, D. F. R.; Orlando, T. M.; Kimmel, G. A.; La Verne, J. A.; Clark, S. B.; Rosso, K. M., Boehmite and Gibbsite Nanoplates for the Synthesis of Advanced Alumina Products. *ACS Appl. Nano Mater.* **2018,** *1*, 7115-7128.

(26) Seyssiecq, I.; Veesler, S.; Pepe, G.; Boistelle, R., The Influence of Additives on the Crystal Habit of Gibbsite. *J. Cryst. Growth* **1999,** *196*, 174-180.

(27) Sweegers, C.; de Coninck, H. C.; Meekes, H.; van Enckevort, W. J. P.; Hiralal, I. D. K.; Rijkeboer, A., Morphology, Evolution and other Characteristics of Gibbsite Crystals Grown from Pure and Impure Aqueous Sodium Aluminate Solutions. *J. Cryst. Growth* **2001,** *233*, 567-582.

(28) Moolenaar, R. J.; Evans, J. C.; Mckeever, L. D., Structure of Aluminate Ion in Solutions at High Ph. *J. Phys. Chem.* **1970,** *74*, 3629-3636.

(29) Pouvreau, M.; Dembowski, M.; Clark, S. B.; Reynolds, J. G.; Rosso, K. M.; Schenter, G. K.; Pearce C. I.; Clark, A. E., Ab Initio Molecular Dynamics Reveal Spectroscopic Siblings and Ion Pairing as New Challenges for Elucidating Prenucleation Aluminum Speciation. *J. Phys. Chem. B.* **2018**, *122*, 7394-7402

(30) Johnston, C. T.; Agnew, S. F.; Schoonover, J. R.; Kenney, J. W.; Page, B.; Osborn, J. Corbin, R. Raman Study of Aluminum Speciation in Simulated Alkaline Nuclear Waste. *Environ. Sci. Technolog.* **2002**, *36*, 2451-2458

(31) Sipos, P.; Hefter, G.; May, P. M., Al-27 NMR and Raman Spectroscopic Studies of Alkaline Aluminate Solutions with Extremely High Caustic Content - Does the Octahedral Species $Al(OH)_6^{3-}$ Exist in Solution? *Talanta* **2006,** *70*, 761-765.

(32) Kass, S. R., Zwitterion-Dianion Complexes and Anion-Anion Clusters with Negative Dissociation Energies. *J. Am. Chem. Soc.* **2005,** *127*, 13098-13099.

(33) Mata, I.; Alkorta, I.; Molins, E.; Espinosa, E., Electrostatics at the Origin of the Stability of Phosphate-Phosphate Complexes Locked by Hydrogen Bonds. *Chemphyschem* **2012,** *13*, 1421-1424.

(34) Mata, I.; Molins, E.; Alkorta, I.; Espinosa, E., The Paradox of Hydrogen-Bonded Anion Anion Aggregates in Oxoanions: A Fundamental Electrostatic Problem Explained in Terms of Electrophilic center dot center dot center dot Nucleophilic Interactions. *J. Phys. Chem. A* **2015,** *119*, 183-194.

(35) Parkhurst, D. L.; Appelo, C. A. J. *User's guide to PHREEQC (Version 2) : A Computer Program for Speciation, Batch-Reaction, One-Dimensional Transport, and Inverse Geochemical Calculations*; 99-4259; 1999.

(36) Zhang, X.; Cui, W.; Hu, J. Z.; Wang, H. W.; Prange, M. P.; Wan, C.; Jaegers, N. R.; Zong, M.; Zhang, H.; Pearce, C. I.; Li, P.; Wang, Z.; Clark, S. B.; Rosso, K. M., Transformation of Gibbsite to Boehmite in Caustic Aqueous Solution at Hydrothermal Conditions. *Cryst. Growth. Des.* **2019**, *19*, 5557-5567.

(37) Stokes, R. H., Isopiestic Vapor Pressure Measurements on Concentrated Solutions of Sodium Hydroxide at 25-Degrees. *J. Am. Chem. Soc.* **1945,** *67*, 1689-1691.

(38) Buchner, R.; Sipos, P.; Hefter, G.; May, P. M., Dielectric Relaxation of Concentrated Alkaline Aluminate Solutions. *J. Phys. Chem. A* **2002,** *106*, 6527-6532.

(39) Smirnov, P. R., Comparative Analysis of Structural Parameters of the Nearest Surrounding of Nitrate and Perchlorate Ions in Aqueous Solutions of Electrolytes. *Russ. J. Gen. Chem.* **2014,** *84*, 1867-1876.

(40) Smirnov, P. R.; Trostin, V. N., Structure of the Nearest Surrounding of the Na^+ Ion in Aqueous Solutions of its Salts. *Russ. J. Gen. Chem.* **2007,** *77*, 844-850.

(41) Vchirawongkwin, S.; Kritayakornupong, C.; Tongraar, A.; Vchirawongkwin, V., Hydration Properties Determining the Reactivity of Nitrite in Aqueous Solution. *Dalton Trans.* **2014,** *43*, 12164-12174.

(42) Vchirawongkwin, V.; Kritayakornupong, C.; Tongraar, A.; Rode, B. M., Symmetry Breaking and Hydration Structure of Carbonate and Nitrate in Aqueous Solutions: A Study by Ab Initio Quantum Mechanical Charge Field Molecular Dynamics. *J. Phys. Chem. B* **2011,** *115*, 12527-12536.

(43) Botti, A.; Bruni, F.; Imberti, S.; Ricci, M. A.; Soper, A. K., Ions in Water: The Microscopic Structure of Concentrated NaOH Solutions. *J. Chem. Phys.* **2004,** *120*, 10154-10162.

(44) Coste, A.; Poulesquen, A.; Diat, O.; Dufreche, J. F.; Duvail, M., Investigation of the Structure of Concentrated NaOH Aqueous Solutions by Combining Molecular Dynamics and Wide-Angle X-ray Scattering. *J. Phys. Chem. B* **2019,** *123*, 5121-5130.

(45) Hellstrom, M.; Behler, J., Concentration-Dependent Proton Transfer Mechanisms in Aqueous NaOH Solutions: From Acceptor-Driven to Donor-Driven and Back. *J. Phys. Chem. Lett.* **2016,** *7*, 3302-3306.

(46) Hellstrom, M.; Behler, J., Proton-Transfer-Driven Water Exchange Mechanism in the Na^+ Solvation Shell. *J. Phys. Chem. B* **2017,** *121*, 4184-4190.

(47) Hellstrom, M.; Behler, J., Structure of Aqueous NaOH Solutions: Insights from Neural-Network-Based Molecular Dynamics Simulations. *Phys. Chem. Chem. Phys.* **2017,** *19*, 82-96.

(48) Mal'tsev, G. Z.; Malinin, G. V.; Mashovets, V. P.; Shcherbakov, V. A., Thermodynamic Properties and H1 and Na23 NMR Spectra of Sodium Hydroxide Solutions. *J. Struct.* **1966,** *6*, 353-358.

(49) Benezeth, P.; Hilic, S.; Palmer, D. A., The Solubilities of Gibbsite and Bayerite Below 100 A degrees C in Near Neutral to Basic Solutions. *J Solution Chem* **2016,** *45*, 1288-1302.

(50) Wesolowski, D. J., Aluminum Speciation and Equilibria in Aqueous-Solution .1. The Solubility of Gibbsite in the System Na-K-Cl-OH-$Al(OH)_4$ from 0-Degrees to 100-Degrees-C. *Geochim. Cosmochim. Acta* **1992,** *56*, 1065-1091.

(51) Volf, F. F.; Kuznetsov, S. I., Polytherms in the Al_2O_3-Na_2O-H_2O System. *Zh. Prikl. Khim.* **1955,** *28*, 597.

(52) Fricke, R.; Jucaitis, P., Untersuchungen über die Gleichgewichte in den Systemen $Al_2O_3 \cdot Na_2O \cdot H_2O$ und $Al_2O_3 \cdot K_2O \cdot H_2O$. *Z. Anorg. Allg. Chem* **1930,** *191*, 129-149.

(53) Berecz, E.; Szita, L., Electrochemical Method for Solubility and Dissolution of Solid Compounds - Some Thermodynamic Properties of System $Al(OH)_3$-NaOH-H_2O. *Electrochim. Acta* **1970,** *15* (8), 1407-1419.

(54) Sipos, P.; May, P. M.; Hefter, G. Quantitative Determination of an Aluminate Dimer in Concentrated Alkaline Aluminate Solutions by Raman Spectroscopy. *Dalton Trans.* **2006**, 368-375

(55) Smith, J. W.; Lam, R. K.; Shih, O.; Rizzuto, A. M.; Prendergast, D.; Saykally, R. J., Properties of Aqueous Nitrate and Nitrite from X-ray Absorption Spectroscopy. *J. Chem. Phys.* **2015**, *143*